L_3-subshell vacancy state alignment in photon-atom collisions

K. S. Kahlon, N. Singh, R. Mittal, K. L. Allawadhi, and B. S. Sood
Nuclear Science Laboratories, Physics Department, Punjabi University, Patiala 147002, India
(Received 22 October 1990)

The differential cross sections for the emission of Ll, $L\alpha_2$, $L\alpha$, $L\beta$, and $L\gamma$ groups of L x-ray lines induced in Au by 59.57-keV photons have been measured at different angles varying from 40° to 120° at intervals of 10°. The $L\alpha_2$ line has been isolated by using preferential absorption of the $L\alpha$ line in a Zn absorber of suitable thickness. The L x rays represented by the Ll, $L\alpha_2$, and $L\alpha$ peaks are found to be anisotropic in the spatial distribution while those in the $L\beta$ and $L\gamma$ peaks are isotropic. The Ll peak has greater anisotropy than the $L\alpha$ peak. The anisotropy of $L\alpha_2$ line is opposite to that of $L\alpha_1$ line. The present results contradict the predictions of Cooper and Zare [*Atomic Collision Processes* (Gordon and Breach, New York, 1969)], that the vacancy state produced after photoionization is not aligned irrespective of its J value, but confirm those of Flugge, Mehlhorn, and Schmidt [Phys. Rev. Lett. **29**, 7 (1972)] that the vacancy state with $J > \frac{1}{2}$ is aligned.

1990 PACS number(s): 32.80.Fb, 32.30.−r

INTRODUCTION

The theoretical predictions of Cooper and Zare [1] and Flugge, Mehlhorn, and Schmidt [2] for the angular distribution of fluorescent x rays emitted after photoionization of inner-shell electrons are contradictory and need experimental verification. The calculations of Cooper and Zare [1] predict that after photoionization the inner-shell vacancy state is not aligned, irrespective of the value of its angular momentum, and the emission of fluorescent x rays consequent to its decay is isotropic. However, later calculations of Flugge, Mehlhorn, and Schmidt [2] do not fully confirm this expectation but show that if angular momentum J of the vacancy state is greater than $\frac{1}{2}$, it is aligned and the resulting x-ray emission is anisotropic. Thus, according to Flugge, Mehlhorn, and Schmidt [2] only those fluorescent x rays that originate from the decay of vacancy states in K, L_1, L_2, M_1, and M_2 subshells with $J=\frac{1}{2}$ will be isotropically emitted, but those from L_3, M_3, and M_4 subshells with $J=\frac{3}{2}$ and from the M_5 subshell with $J=\frac{5}{2}$ will show anisotropic spatial distribution. In order to test theoretical calculations, we have measured the differential cross sections for the emission of Ll, $L\alpha$, $L\beta$, and $L\gamma$ groups of L x rays of Au by 59.57-keV γ rays at different angles ranging from 40° to 120° at intervals of 10°. We have also made an effort to obtain information about the angular distribution of the $L\alpha_2$ line separately by isolating it with a thin Zn absorber that absorbs the $L\alpha_1$ line preferentially. The experimental setup, method of measurement, and results are reported in this paper.

EXPERIMENTAL SETUP AND METHOD OF MEASUREMENT

The experimental arrangement used in the present measurements was similar to the one used earlier [3] and is shown in Fig. 1. Briefly, an ^{241}Am source, Au target, and Si(Li) detector were arranged on a graduated turntable so that the source and target could be moved together with respect to the detector, which was kept fixed at one position. The shielding was arranged so that the 59.57-keV γ rays emitted from the ^{241}Am source of strength of approximately 100 mCi were made to fall on a 99.99% pure metallic Au target of thickness 40 mg/cm^2. The radiation emitted from the target at an angle θ after the interaction of γ rays with it was collimated on the Si(Li) detector (effective area, 200 mm^2; thickness, 5 mm; Be window thickness, 0.05 mm) coupled to a Nuclear Data Inc. 76 multichannel analyzer system. The resolution of the x-ray spectrometer was approximately 180 eV

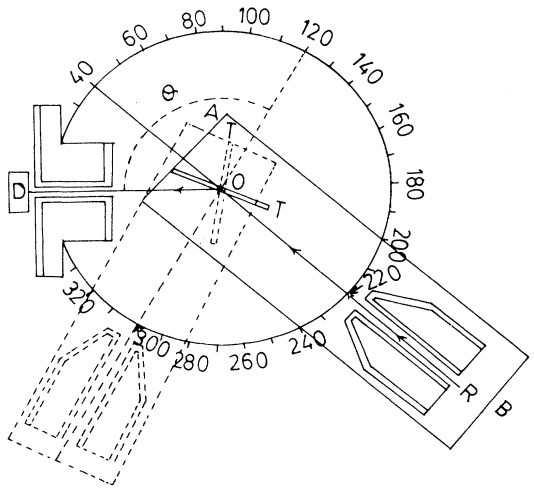

FIG. 1. Experimental setup used to measure the differential cross sections for the emission of L-subshell x rays of Au. R is the ^{241}Am source, T is the gold target, and D is the Si(Li) detector. R and T are mounted on a movable arm AB capable of rotation about an axis through the center 0 of a graduated circular turntable.

at 5.9 keV. The angle of incidence was kept fixed at 70° while the angle θ at which the radiation emitted from the target was detected was varied from 40° to 120° with an angular spread of 2.5° by moving the source and target together with respect to the detector A signal-to-background ratio of 1000:1 was obtained by a suitable adjustment of the sizes of the collimators and distances of the source and the detector from target. The radiation emitted from target and falling on the detector consisted mainly of L-, M-, and higher-shell fluorescent x rays characteristic of Au and coherent and incoherent scattering of 59.57-keV γ rays. Since K-shell electrons of the Au target were not excited by 59.57-keV γ rays there was no transfer of vacancies from the K to the L shell. The emission of L-shell x rays from the target was thus entirely due to photoionization of L-shell electrons. In case any alignment of L-subshell vacancy states was produced by photoionization, it was not disturbed due to the transfer of vacancies from the K shell to the L subshells. However, the alignment of L_3-subshell vacancy states with $J=\frac{3}{2}$ if it is produced after photoionization would be affected by the transfer of vacancies from the L_1 and L_2 subshells with $J=\frac{1}{2}$ through Coster-Kronig transitions. As a consequence of the transfer of vacancies from the L_1 and L_2 subshells to the L_3 subshell, the emission of x rays from the L_3 subshell would be enhanced by a factor K defined as

$$K=\frac{\sigma_3+\sigma_2 f_{23}+\sigma_1(f_{13}+f_{12}f_{23})}{\sigma_3}\ , \tag{1}$$

where σ_1, σ_2 and σ_3 are the L_1-, L_2-, and L_3-subshell photoionization cross sections and f_{ij} are the Coster-Kronig transition probabilities from the i to the j subshell. In the present measurements, the value of the enhancement factor K, when calculated by using the interpolated theoretical values of Scofield [5] for σ_1, σ_2 and σ_3 for Au at 59.57 keV and the semiempirical values of Krause [6] for f_{12}, f_{13}, and f_{23} for Au, is found to be 1.92. The x-ray emission due to the filling of the L_3-subshell vacancies produced only by the photoionization of L_3-subshell electrons is thus 52% of the L_3-subshell x rays actually observed in the present measurements.

The L-shell x rays are easily separated from the M- and higher-shell x rays, as well as the coherent and incoherent γ-ray scattering by the Si(Li) detector used in the present measurements. The contribution of $L\alpha_2$ line to the $L\alpha$ peak was determined by placing the 21.57-mg/cm^2-thick Zn absorber in front of the detector. The absorber took in 99.98% of $L\alpha_1$ line while it transmitted 43% of the $L\alpha_2$ line. Typical L x-ray spectra taken at an emission angle of 90° without, and with, the Zn absorber are shown in Figs. 2(a) and 2(b), respectively. Ll, $L\alpha$, $L\beta$ and $L\gamma$ peaks of Au are resolved in the spectrum obtained without the absorber [Fig. 2(a)]. In the spectrum with the Zn absorber shown in Fig. (2b), the Ll line of Au is not seen because it is almost completely absorbed in the absorber. However, the $K\alpha$ line of Zn appears on the lower-energy side of the $L\alpha_2$ peak of Au, but the $K\beta$ line of Zn merges with it. All the peaks in Figs. 2(a) and 2(b) are labeled and explained in the captions of the figures.

From the measurement of counts under the Zn $K\alpha$ peak and the known ratio of $I(K\alpha)/I(K\beta)$, the contribution of the Zn $K\beta$ line to the $L\alpha_2$ peak was estimated to be 9%.

The differential cross section for the emission of L x rays under the Li peak ($i=l,\alpha_2,\alpha,\beta,\gamma$) at an angle θ is given by

$$\frac{d\sigma_{Li}(\theta)}{d\Omega}=N_{Li}(\theta)\frac{M}{N}\frac{1}{t}\frac{1}{\beta_{Li}(\theta)}\frac{4\pi}{S_\gamma a_\gamma \omega_1\omega_2(\theta)\epsilon_{Li}(\theta)}\ , \tag{2}$$

where $N_{Li}(\theta)$ is the number of L x rays detected per second in the Li x-ray peak at an angle θ with the incident γ-ray beam. M is the atomic weight of Au in g, N is Avogadro's number, t is the thickness of the target in g/cm^2, $\beta_{Li}(\theta)$ is the target self-absorption correction fac-

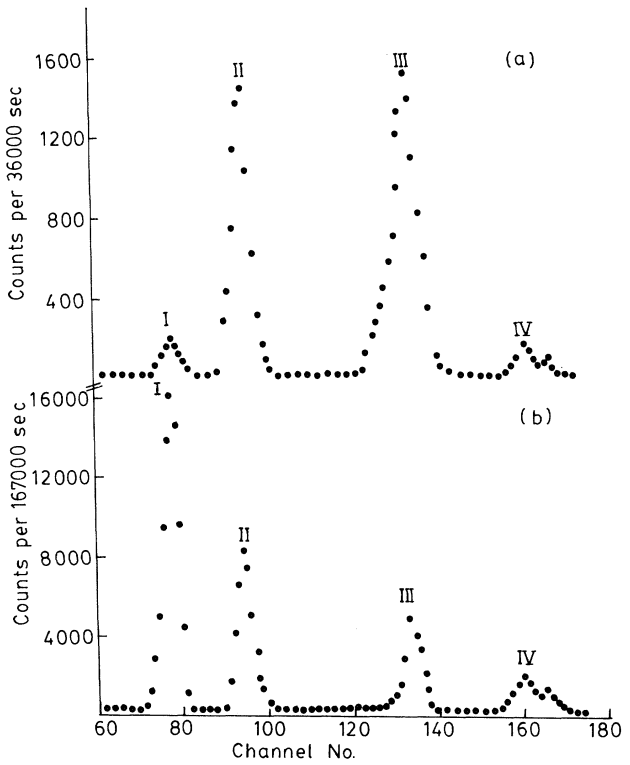

FIG. 2. Spectrum of Au L x rays emitted at 90°. Peaks I, II, III, and IV correspond to Ll, $L\alpha$, $L\beta$, and $L\gamma$ groups of L x-ray-emission lines of Au, respectively. (b) Spectrum of Au L x rays emitted at 90° after absorption in the Zn absorber placed in front of the detector. Peaks I, II, III, and IV correspond to the $K\alpha$ x rays of Zn, $K\beta$ x rays of Zn, and $L\alpha$ x rays of Au, $L\beta$ x rays of Au; and $L\gamma$ x rays of Au, respectively. Ll x rays of Au are almost completely absorbed in the Zn absorber, while the intensities of $L\alpha$, $L\beta$, and $L\gamma$ x rays of Au are reduced due to absorption in the Zn absorber. Peaks due to $K\alpha$ and $K\beta$ x rays of Zn appear in the spectrum. $K\beta$ x rays of Zn merge in the $L\alpha_2$ peak of Au and give rise to composite peak II.

tor, which takes into account the absorption of incident γ rays and emitted x rays in the target. S_γ is the number of 59.57-keV γ rays emitted per second from the source, ω_1 and $\omega_2(\theta)$ are the source-target and target-detector solid angles, a_γ is the correction factor due to absorption of γ rays in the air column between the source and target, $\epsilon_{Li}(\theta)$ is the efficiency of the detector for the detection of x rays emitted at angle θ in the Li x-ray peak, ω_1 is independent of θ since the angle of incidence is kept fixed throughout the experiment, but $N_{Li}(\theta)$, $\beta_{Li}(\theta)$, $\omega_2(\theta)$, and $\epsilon_{Li}(\theta)$ are dependent on θ. Therefore, for the measurement of differential x-ray emission cross sections, the values of $N_{Li}(\theta)$, $\beta_{Li}(\theta)$, $\omega_2(\theta)$, and $\epsilon_{Li}(\theta)$ have to be determined at each of the angles θ. $N_{Li}(\theta)$ was measured from the total number of counts per unit time for the various peaks observed in the L x-ray spectra taken at various angles. The terms $(M/N)(1/t)$ and $\beta_{Li}(\theta)$ were calculated from the physical parameters of the target and the absorption coefficients of incident γ rays and emitted x rays in Au, respectively. Since the emitted x rays for each of the Li peaks consist of a number of x-ray lines of distinct energies and intensities, the value of $\beta_{Li}(\theta)$ at different angles of emittance used in the experiment were calculated by the procedure described earlier [4]. The values of the factor $4\pi/S_\gamma a_\gamma \omega_1 \omega_2(\theta)\epsilon_{Li}(\theta)$, which contains terms relating to γ-ray source strength, source-target, and target-detector solid angles, and detector efficiency were determined experimentally for various emission angles and different x-ray energies ranging from 6 to 26 keV in terms of K x-ray production cross sections, which are known to an accuracy of approximately 1%.

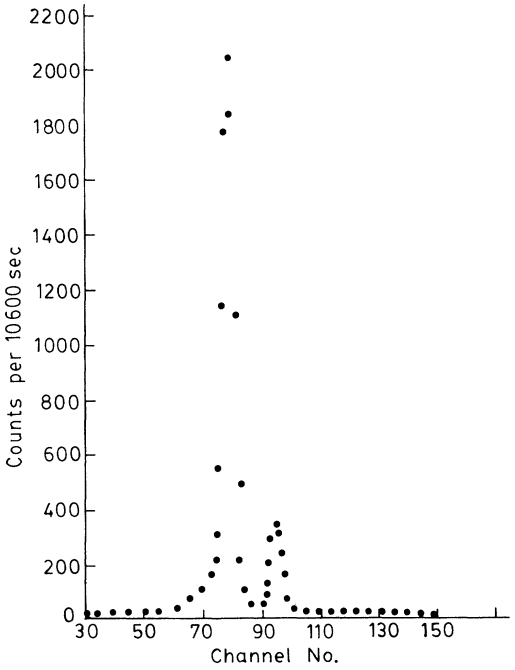

FIG. 3. Spectrum of Zn K x rays emitted at 90°.

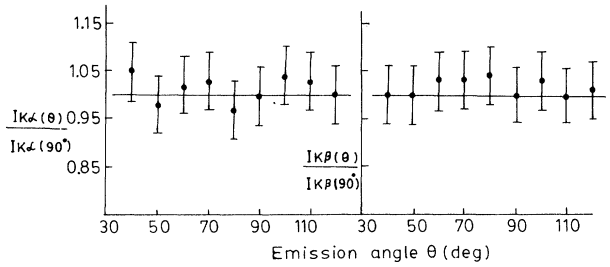

FIG. 4. Relative intensity ratios of $I_{K\alpha}(\theta)/I_{K\alpha}(90°)$ and $I_{K\beta}(\theta)/I_{K\beta}(90°)$ of Gd, $K\alpha$ and $K\beta$ x-ray lines at different emission angles.

To obtain this, the Au target was replaced, in turn, with targets of Fe, Ni, Zn, Ge, Se, Y, Zr, Mo, Ag, and Sn having the same diameter as that of the Au target, and the intensity of the K x rays emitted from each of the targets at different angles was recorded. A typical spectrum of K x rays emitted from the target of Zn at 90° is shown in Fig. 3. It can be easily seen that the factor under reference,

$$\frac{4\pi}{S_\gamma a_\gamma \omega_1 \omega_2(\theta)\epsilon_{Li}(\theta)} = \frac{\sigma_K}{4\pi}\frac{1}{N_K(\theta)}\frac{N}{M}t_K\beta_K(\theta)\,, \quad (3)$$

where various terms have the same meaning as those explained in Eq. (1) but correspond to the K shell, was evaluated as explained above. Isotropic emission of K x-rays, which has also been verified experimentally by us, is assumed. The intensity ratio $I_{Ki}(\theta)/I_{Ki}(90°)$ $(i=\alpha,\beta)$ of K x rays of Gd excited by 59.57-keV γ rays measured at different angles in the experimental setup described above is shown in Fig. 4. The intensity ratio is found to be independent of the angle of emission, which shows that the

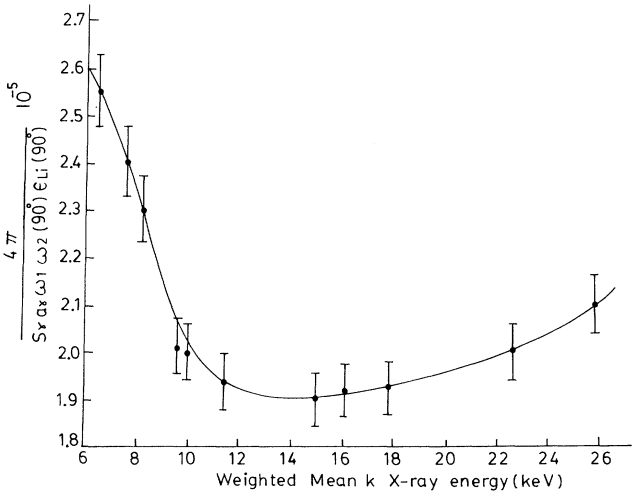

FIG. 5. Values of the factor $[4\pi/S_\gamma a_\gamma \omega_1 \omega_2(90°)\epsilon_{Li}(90°)]$ at weighted mean K x-ray energies of elements $26 \leq Z \leq 50$.

TABLE I. Measured differential Li x-ray emission cross sections, $i=(l,\alpha_2,\alpha,\beta,\gamma)$.

Angle of emission θ	$\frac{d\sigma_{Ll}(\theta)}{d\Omega}$	$\frac{d\sigma_{L\alpha_2}(\theta)}{d\Omega}$	$\frac{d\sigma_{L\alpha}(\theta)}{d\Omega}$	$\frac{d\sigma_{L\beta}(\theta)}{d\Omega}$	$\frac{d\sigma_{L\gamma}(\theta)}{d\Omega}$
40°	0.80±0.06	0.87±0.05	12.9±0.9	11.9±0.6	2.07±0.15
50°	0.72±0.05	0.98±0.06	12.5±0.9	12.2±0.6	1.99±0.15
60°	0.68±0.06	1.03±0.06	12.0±0.9	12.3±0.6	2.23±0.17
70°	0.65±0.05	1.16±0.07	11.7±0.8	11.8±0.6	2.23±0.17
80°	0.60±0.04	1.24±0.07	11.5±0.8	11.9±0.6	2.31±0.17
90°	0.56±0.04	1.28±0.07	11.2±0.8	11.9±0.6	2.07±0.15
100°	0.51±0.04	1.34±0.08	10.7±0.8	12.0±0.6	2.15±0.16
110°	0.48±0.04	1.32±0.08	10.5±0.7	12.3±0.6	1.99±0.15
120°	0.45±0.03	1.33±0.08	10.1±0.7	12.1±0.6	2.27±0.17

K x-ray emission is isotropic. The values of the factor for different emission angles at the weighted mean energies of the K x rays of the elements of various targets with atomic number $26 \leq Z \leq 50$ were determined from Eq. (3). The values of the factor corresponding to a typical emission angle of 90° is shown in Fig. 5. The values of the factor for various emission angles at different weighted mean energies corresponding to different (Li) x-ray groups of lines were determined from figures similar to Fig. 5 for the evaluation of differential cross sections from Eq. (1).

RESULTS AND DISCUSSION

The measured values of differential cross sections at different emission angles varying from 40° to 120° at intervals of 10° for the emission of Ll, $L\alpha_2$, $L\alpha$, $L\beta$, and $L\gamma$ groups of L x-ray lines are listed in Table I. To the best of our knowledge, no other experimental data are available for comparison with the results obtained by us. The errors in the present measurements are approximately 6–8 %, and are due to the counting of statistics and the uncertainties involved in the measurement and calculation of other parameters used for the determination of x-ray-emission cross sections from Eq. (1).

It is seen from the results that Ll, $L\alpha_2$, and $L\alpha$ peaks show anisotropic emission, while $L\beta$ and $L\gamma$ peaks are emitted isotropically. The anisotropy of the Ll and $L\alpha_2$ peaks is greater than that of the $L\alpha$ peak. The differential cross sections for the emission of the $L\alpha_2$ line increases with emission angle, whereas it decreases for the $L\alpha$ group. Therefore, the anisotropy of the $L\alpha_2$ line is opposite that of the $L\alpha$ group, showing that the $L\alpha_1$ and $L\alpha_2$ components of the $L\alpha$ group have opposite anisotropy. Ll, $L\alpha$, and $L\alpha_2$ peaks originate from the transitions to L_3 subshells ($J=\frac{3}{2}$) only and are thus expected to show anisotropic emission according to the calculations of Flugge, Mehlhorn, and Schmidt [2]. The observed anisotropy of Ll and $L\alpha_2$ peaks is more than that of the $L\alpha$ peak because the Ll and $L\alpha_2$ peaks contain one intense line corresponding to L_3-M_1 and L_3-M_4 transitions, respectively, but the $L\alpha$ peak contains $L\alpha$ L_3-M_5 and $L\alpha_2$ L_3-M_4 lines of opposite anisotropy. The $L\gamma$ peak consists of the transitions from L_1 ($J=\frac{1}{2}$) and L_2 ($J=\frac{1}{2}$) subshells and is thus expected to be isotropically emitted. However, even though the $L\beta$ peak contains some contribution from the L_3 ($J=\frac{3}{2}$) -subshell transition, it does not show any measurable anisotropy because of the presence of other strong transitions from the L_1 ($J=\frac{1}{2}$) and L_2 ($J=\frac{1}{2}$) subshells. Thus, $L\beta$ may also be taken to be isotropically emitted within the uncertainties of present measurements.

Representing the differential x-ray emission cross sections for any group Li of the L x-ray lines by a Legendre polynomial sum,

$$\frac{d\sigma_{Li}(\theta)}{d\Omega}=\sum_l a_l P_l(\cos\theta) ,$$

the observed cross-sections are fitted to the relation

$$\frac{d\sigma_{Li}(\theta)}{d\Omega}=a_0+a_1\cos\theta+a_2\cos^2\theta . \quad (4)$$

TABLE II. Experimental values of coefficients a_n, $n=0,1,2$.

Coefficients a_n	Ll	$L\alpha_1$	$L\alpha$	$L\beta$	$L\gamma$
a_0	0.56	1.28	12.0	11.5	2.15
a_1	0.20	−0.088	1.87	0	0
a_2	0.08	−0.584	−0.54	0	0

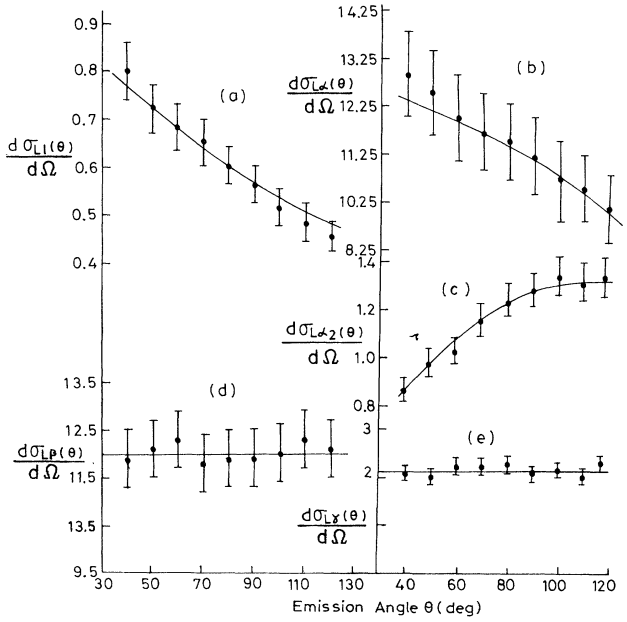

FIG. 6. The differential L-shell x-ray-emission cross sections of Au at angles from 40° to 120°. (a) $d\sigma_{Ll}(\theta)/d\Omega$ vs θ. (b) $d\sigma_{L\alpha}(\theta)/d\Omega$ vs θ. (c) $d\sigma_{L\alpha_2}(\theta)/d\Omega$ vs θ. (d) $d\sigma_{L\beta}(\theta)/d\Omega$ vs θ. (e) $d\sigma_{L\gamma}(\theta)/d\Omega$ vs θ.

The values of the coefficients a_0, a_1, and a_2 are listed in Table II. The experimental values of differential cross sections and the fitted curves are shown in Fig. 6. The observed anisotropy of the Ll, $L\alpha_2$, and $L\alpha$ groups of L x-ray lines contradicts the predictions of Cooper and Zare [1] that after photoionization the vacancy state is not aligned, but confirms those of Flugge, Mehlhorn, and Schmidt [2] that the vacancy state with $J > \frac{1}{2}$ is aligned.

Since theoretical values of the angular distribution functions for the emission of the Ll, $L\alpha_2$, and $L\alpha$ groups of lines are not available in the literature, integral cross sections were determined from the measured angular distribution coefficients (a_n) for comparison with theory using the relation

TABLE III. Li x-ray-emission integral cross sections.

Li x-ray group	Experimental values of coefficients a using relation (5)	Theoretical relations (6)–(10)
Ll	7.4±0.5	7.3
$L\alpha_2$	13.6±0.8	14.1
$L\alpha$	138±7	142
$L\beta$	144.5±4.5	149
$L\gamma$	27±1	26.5

TABLE IV. Experimental values of coefficients b_n, $n = 0, 1, 2$.

Coefficients b_n	Ll	$L\alpha_2$	$L\alpha$
b_0	0.29	0.73	5.6
b_1	0.24	−0.24	2.04
b_2	0.02	−0.36	0.03

$$\sigma_{Li} = 2\pi \int_0^{\pi} \sum_{n=0}^{2} a_n \cos^n\theta \sin\theta \, d\theta \ . \tag{5}$$

In Table III, the values of the integral cross sections for the emission of the Ll, $L\alpha_2$, $L\alpha$, $L\beta$, and $L\gamma$ groups of L x-ray lines, as determined above, are compared with those calculated from the following relations:

$$\sigma_{Ll} = [\sigma_1(f_{13} + f_{12}f_{23}) + \sigma_2 f_{23} + \sigma_3]\omega_3 F_{3l} \ , \tag{6}$$

$$\sigma_{L\alpha_2} = [\sigma_1(f_{13} + f_{12}f_{23}) + \sigma_2 f_{23} + \sigma_3]\omega_3 F_{3\alpha_2} \ , \tag{7}$$

$$\sigma_{L\alpha} = [\sigma_1(f_{13} + f_{12}f_{23}) + \sigma_2 f_{23} + \sigma_3]\omega_3 F_{3\alpha} \ , \tag{8}$$

$$\sigma_{L\beta} = \sigma_1\omega_1 F_{1\beta} + (\sigma_2 + \sigma_1 f_{12})\omega_2 F_{2\beta} + [\sigma_3 + \sigma_2 f_{23} + \sigma_1(f_{13} + f_{12}f_{23})]\omega_3 F_{3\beta} \ , \tag{9}$$

$$\sigma_{L\gamma} = \sigma_1\omega_1 F_{1\gamma} + (\sigma_2 + \sigma_1 f_{12})F_{2\gamma} \ , \tag{10}$$

where ω_1, ω_2, and ω_3 are L_1-, L_2-, and L_3-subshell fluorescence yields and F_{3l} is the fraction of intensity of x rays originating from L_3 transitions, which contribute to the Ll peak of L x-ray spectrum. All other F's are similarly defined. Other terms have already been defined in Eq. (1). It is seen that the measured values agree fairly well with the calculated values, showing the validity of the method used to determine the angular distribution coefficients a_n.

The effect on the alignment of the L_3-subshell vacancy states produced by direct photoionization of the L_3 subshell, due to transfer of vacancies to the L_3 subshell from

TABLE V. Ratios of coefficients a_1/a_0 and b_1/b_0 for Ll $L\alpha_2$, and $L\alpha$ lines, with use of the Legendre polynomial representing x-ray emission of Eqs. (4) and (11).

X-ray lines	a_1/a_0 with Coster-Kronig transitions	b_1/b_0 without Coster-Kronig transitions
Ll	0.36	0.81
$L\alpha_2$	−0.07	−0.32
$L\alpha$	0.16	0.36

TABLE VI. Integral cross sections determined from the measured angular distribution coefficients a_n and b_n for Ll and $L\alpha$ x-ray-emission lines and enhancement factor K from their ratios.

X-ray lines	Integral cross sections origin: Eq. (5) using coefficients a_n with Coster-Kronig transitions σ_{Li}	Eq. (12) using coefficients b_n without Coster-Kronig transitions σ^p_{Li}	Enhancement factor: Experimental $=\sigma_{Li}/\sigma^p_{Li}$	Theory from Eq. (1)
Ll	7.4±0.5	3.7±0.3	2±0.21	1.92
$L\alpha$	138±7	71±5	1.94±0.17	1.92

the L_1 and L_2 subshells through Coster-Kronig transitions, was investigated by determining the differential cross section $d\sigma^p_{Li}(\theta)$ for the emission of Ll, $L\alpha_2$, and $L\alpha$ lines at different angles due to the filling of L_3-subshell vacancies produced by direct photoionization of the L_3-subshell electrons only. If it is assumed that the vacancies transferred from the L_1 and L_2 subshells to the L_3 subshell are not aligned and thus the emission of x rays subsequent to the filling of transferred vacancies is isotropic, the differential cross sections $d\sigma^p_{Li}(\theta)$ at various angles are determined by subtracting the calculated values of

$$[\sigma_2 f_{23}+\sigma_1(f_{13}+f_{12}f_{23})]\omega_3 F_{3i}/4\pi$$

(the contribution due to transferred vacancies) from the measured values of $d\sigma_{Li}(\theta)$ at those angles. The differential cross sections $d\sigma^p_{Li}(\theta)$ are then fitted to the relation

$$\frac{d\sigma^p_{Li}(\theta)}{d\Omega}=b_0+b_1\cos\theta+b_2\cos^2\theta\ , \tag{11}$$

which is similar to relation (4), discussed above. The values of the coefficients b_0, b_1, and b_2, thus determined, are listed in Table IV.

The ratio of the coefficients a_1/a_0 for the Ll, $L\alpha_2$, and $L\alpha$ lines obtained from the cross sections $d\sigma_{Li}(\theta)/d\Omega$ containing contributions of the Coster-Kronig transitions transferring vacancies from the L_1 and L_2 subshells to the L_3 subshell and the ratio of coefficients b_1/b_0 obtained from cross sections $d\sigma^p_{Li}(\theta)/d\Omega$ without the contribution of the Coster-Kronig transitions are listed in Table V. It is seen that the value of $|a_1/a_0|$ is less than that of $|b_1/b_0|$ for each of the Ll, $L\alpha_2$, and $L\alpha$ x-ray lines, showing that the spatial anisotropy of the lines originating from the L_3 subshell is reduced by the transfer of vacancies from the L_1 and L_2 subshells to the L_3 subshell through the Coster-Kronig transitions. This reduction in spatial anisotropy may be interpreted on the basis of the conclusions drawn earlier in the text that the vacancies created after photoionization in the L_3 subshell with $J=\frac{3}{2}$ are aligned, and those created in the L_1 and L_2 subshells with $J=\frac{1}{2}$ are not aligned. The overall anisotropy in the emission of x rays originating from the filling of vacancies in the L_3 subshell is reduced after some unaligned vacancies from the L_1 and L_2 subshells are transferred to join the aligned vacancies in the L_3 subshell produced by direct photoionization of the L_3-subshell electrons, provided the transfer of vacancies to the L_3 subshell takes place before x-ray emission from it. From the observed decrease in the spatial anisotropy of Ll, $L\alpha_2$, and $L\alpha$ lines it may be safely concluded that the Coster-Kronig transitions are faster than x-ray emission from the L shell.

In order to provide another check on the correctness of the procedure used in the above investigations, the integral cross sections for the emission of the Ll and $L\alpha$ lines σ^p_{Li} without the Coster-Kronig transitions were determined from the measured angular distribution coefficients by using the relation

$$\sigma^p_{Li}=2\pi\int_0^\pi \sum_{n=0}^{2} b_n\cos^n\theta\sin\theta\, d\theta \tag{12}$$

and compared with the σ_{Li} determined from the measured angular distribution coefficients a_n, which takes into account the Coster-Kronig transitions to obtain the enhancement factor K for the emission of L x rays originating from the L_3 subshell due to the transfer of vacancies from the L_1 and L_2 subshells to the L_3 subshell through the Coster-Kronig transitions. These results are summarized in Table VI.

The experimental values of the enhancement factors for both the Ll and $L\alpha$ lines are found to compare favorably with the theoretically calculated values. Good agreement between the experimental and theoretical values of the enhancement factor confirms that the procedure used in the above investigations is correct.

ACKNOWLEDGMENTS

Financial support from Department of Science and Technology, India, and University Grants Comission, India, is gratefully acknowledged.

[1] J. Cooper and R. N. Zare, *Atomic Collision Processes* (Gordon and Breach, New York, 1969), Vol. XIC, p. 317.
[2] S. Flugge, W. Mehlhorn, and V. Schmidt, Phys. Rev. Lett. **7**, 29 (1972).
[3] K. S. Kahlon, K. Shatindra, K. L. Allawadhi, and B. S. Sood, Pramana J. Phys. **35**, 105 (1990).
[4] S. K. Arora, K. L. Allawadhi, and B. S. Sood, J. Phys. B **14**, 1423 (1981).
[5] J. H. Scofield, Lawrence Livermore Laboratory Report No. UCRL-51326, 1973 (unpublished).
[6] M. O. Krause, J. Phys. Chem. Ref. Data **8**, 307 (1979).